processes

MDPI

Article

Design and Optimization of a Wave-Adaptive Mechanical Converter for Renewable Energy Harvesting Along NEOM's Surf Coast

Abderraouf Gherissi [1,*], Ibrahim Elnasri [1], Abderrahim Lakhouit [2] and Malek Ali [3]

[1] Department of Mechanical Engineering, Faculty of Engineering, University of Tabuk, Tabuk 47913, Saudi Arabia; inasri@ut.edu.sa
[2] Department of Civil Engineering, Faculty of Engineering, University of Tabuk, Tabuk 47913, Saudi Arabia; a.lakhouit@ut.edu.sa,
[3] Aircraft Maintenance Department, Faculty of Aviation Sciences, Amman Arab University, Amman 11953, Jordan; m.alsalem@aau.edu.jo
* Correspondence: a.gresi@ut.edu.sa; Tel.: +966-543440530

Abstract

This study introduces a novel adaptive Mechanical Wave Energy Converter (MWEC) designed to efficiently capture nearshore wave energy for sustainable electricity generation along the southeast surf coast of NEOM (135° longitude). The MWEC system features a polyvinyl chloride (PVC) cubic buoy integrated with a mechanical power take-off (PTO) mechanism, optimized for deployment in shallow waters for a depth of around 1 m. Three buoy volumes, V1: 6000 cm^3, V2: 30,000 cm^3, and V3: 72,000 cm^3, were experimentally evaluated under consistent PTO and spring tension configurations. The findings reveal a direct relationship between buoy volume and force output, with larger buoys exhibiting greater energy capture potential, while smaller buoys provided faster and more stable response dynamics. The energy retention efficiency of the buoy–PTO system was measured at 20% for V1, 14% for V2, and 10% for V3, indicating a trade-off between responsiveness and total energy capture. Notably, the largest buoy (V3) generated a peak power output of 213 W at an average wave amplitude of 65 cm, confirming its suitability for high-energy conditions along NEOM's surf coast. In contrast, the smaller buoy (V1) performed more effectively during periods of reduced wave activity. Wave climate data collected during November and December 2024 support a hybrid deployment strategy, utilizing different buoy sizes to adapt to seasonal wave variability. These results highlight the potential of modular, wave-adaptive mechanical systems for scalable, site-specific renewable energy solutions in coastal environments like NEOM. The proposed MWEC offers a promising path toward low-cost, low-maintenance wave energy harvesting in shallow waters, contributing to Saudi Arabia's sustainable energy goals.

Keywords: wave energy harvesting; adaptive MWEC; PVC cubic buoy; NEOM surf zone; shallow-water converter; Red Sea renewable energy

Academic Editor: Michael C. Georgiadis

Received: 3 September 2025
Revised: 30 September 2025
Accepted: 8 October 2025
Published: 10 October 2025

Citation: Gherissi, A.; Elnasri, I.; Lakhouit, A.; Ali, M. Design and Optimization of a Wave-Adaptive Mechanical Converter for Renewable Energy Harvesting Along NEOM's Surf Coast. *Processes* **2025**, *13*, 3229. https://doi.org/10.3390/pr13103229

1. Introduction

Neom city in Saudi Arabia has an extensive coastline along the Red Sea that provides continuous and highly active wave conditions. The main shoreline orientations are the southeast coast (135°) and the northwest coast (315°). Wave energy is one of the available clean energy resources in Neom. Sea waves play an important role in meeting the increasing electricity demand in many coastal cities worldwide [1].

Neom projects face several challenges, particularly the scarcity of natural resources such as water and clean energy. To address these challenges, Neom requires the exploitation of renewable energy resources, including solar, wind, and wave energy, to meet future power demands. Several studies have discussed the sustainability of Neom in this context [2,3]. One of Neom's central objectives is to become a sustainable city, and investment in renewable resources is essential to achieve this goal.

Wave energy has been recognized as a renewable energy source since 1991 by the European Commission, which integrated it into its renewable energy program. By 1992, several official projects began across European countries. Research and development efforts in Norway started as early as 1975, and by 1985, two shoreline wave energy converters (WECs) were already installed [4]. In the United States and Canada, multiple projects were launched after 2007. In Saudi Arabia, particularly in the Neom region, wave energy converters still represent an opportunity for research, development, and the proposal of suitable designs that can match the wave conditions of the Red Sea and provide optimal clean electricity generation.

The choice of an appropriate WEC design for Neom requires evaluating the existing WEC technologies. Several wave energy conversion technologies are available in the literature and real-world applications. The most suitable design depends on the wave characteristics of a specific location. Wave type and local hydrodynamic behavior are key in selecting the right WEC. Based on several studies [4–6]. WECs can be classified into different groups: shoreline, breakwater, and floating devices. The following includes some examples:

Attenuator WECs are long floating structures composed of segments connected by flexible joints, aligned parallel to incoming waves. Their oscillatory movement is converted into electricity using generators. Examples include Pelamis [7–11] and Wave Star [12–14].

Point absorbers consist of buoys floating on the water surface, moored to the seabed, and oscillating vertically with waves. Their motion drives generators through mechanical or hydraulic PTO systems. Examples include OPT Power Buoy [15], Aqua Buoy [16–18], Archimedes Buoy [19,20], Uppsala WEC [21,22], Wave Bob [23,24], Wave Roller [25,26], Bio Wave [27,28], and Pendulum WEC [29–31].

Oscillating Water Column (OWC) WECs convert wave-induced air pressure variations inside a chamber into rotational energy using turbines. Designs include Limpet [32], Pico Plant [33,34], Mighty Whale [35–37], Osprey [38], and Scanline systems [39].

Overtopping WECs capture waves in elevated reservoirs and release the collected water through turbines. Examples include TAPCHAN [40–43] and Wave Dragon [44].

The success of WEC deployment also depends on wave behavior and site selection. Several studies have investigated Red Sea wind and wave patterns using meteorological models [45]. The Neom coastline, located in the north of the Red Sea, has one of the highest nearshore potentials with approximately 3 kW/m of wave power and 500 W/m of wind power [6]. The identification of optimal installation sites is, therefore, critical.

Wave height measurement is essential for WEC design and energy prediction. Wave energy depends primarily on wave height. Models such as WAVEWATCH III and SWAN simulate wave conditions under various inputs. For example, the work of Hwang et al. [46] measured wave height using a convolutional neural network combined with ocean wave images. Red Sea studies by Sabique Langodan et al. [47] divide the basin into northern, central, and southern regions. In the northern Red Sea near Neom, waves are generated by winds blowing from the northern end and narrow jets from the Arabian side. Ahmed I. et al. [48] analyzed Red Sea wave climatology from 1959 to 2022 and reported significant wave heights (Hs) ranging from 0.5 to 3 m (mean 0.8 m) and mean wave periods (Tm)

between 3.1 and 7 s (annual mean 4 s). Longer-period waves are common near Neom, close to the Gulfs of Suez and Aqaba.

Another major challenge is the PTO system. WECs operate under harsh marine conditions with random waves, high salinity, and difficult access for maintenance. The PTO system must be reliable, robust, and cost-effective. PTO design strongly influences overall WEC cost, sometimes reaching 30% of the total [49]. Different WEC types use different PTO systems: OWC devices employ air turbines, while point absorbers typically use mechanical or hydraulic PTOs [50].

The optimization of hydraulic PTO design and control remains a key challenge for improving energy capture. Recent studies also emphasize the need for accurate modeling of wave evolution and hydrodynamic processes to estimate maximum wave heights and surface power [51]. Simulation-based studies such as the work of Ahmed I. et al. [48] and datasets such as the Global Forecast System (GFS) from Aquilink [52] support long-term wave characterization. Also the work of Misaa Alkhayyat et al. [6] analyzed eight locations at depths between 21.5 m and 55.4 m, reporting significant wave heights of 0.54–0.79 m and wave periods of 3.5–4 s.

Based on the available wave resources, this study proposes a new Mechanical Wave Energy Converter (MWEC) for deployment in the surf zone along Neom's southeast coast (135°). The MWEC incorporates PVC cubic buoys of three different volumes coupled with a mechanical PTO. The experimental results from these buoy types are presented and compared to evaluate performance and suitability for the Neom Red Sea conditions.

2. Materials and Methods

The main component of the MWEC that interacts with waves is the buoy. For this study, PVC buoys were selected due to their light weight, low cost, and widespread market availability. The design concept of the MWEC focuses on developing a low-cost wave energy converter suitable for shallow-water installation, with flexibility to adjust the power take-off (PTO) system, modify buoy volume, control the impact angle with waves, and regulate buoy height. The entire MWEC assembly is mounted on a metallic frame fixed to the seabed (Figure 1). As incoming waves lift the floating buoy (3), the attached toothed gear rack (2) moves upward (Figure 1). This translational motion drives the gear (7) to rotate clockwise during the buoy's ascent. Gear (7) is connected to shaft (12), which is supported horizontally by two ball-bearing blocks. A pulley (13) is mounted on the same shaft to transmit rotational motion via a belt to an electrical generator (Figure 2). To stabilize the rotary dynamics, a flywheel (6) is also fixed to the shaft. The rack slot (2) and chain (14) are attached to the buoy's center. As the buoy oscillates with the waves, two ball bearings and guiding slots constrain its movement to translation (Figure 3). Wave power transmission occurs during the upward motion through the pinion gear (7), while a spring (8) attached to the external frame restores the buoy to its downward position. The shaft (12), through the pulley–belt system, continuously transfers the rotation to the generator, enabling electricity production.

The cubic buoy geometry (Figure 3) was chosen for this prototype because it offers more consistent motion compared to the commonly used spherical or cylindrical buoys, while also reducing vortex formation and induced drag. Its flat, well-defined waterplane area supports stable and repeatable movement of the MWEC.

Several studies have reported that energy extraction efficiency decreases when using different buoy shapes and various PTO systems [53]. To address this, a prototype was developed to experimentally evaluate different buoy volumes with a mechanical PTO system using a cubic buoy (Figure 4).

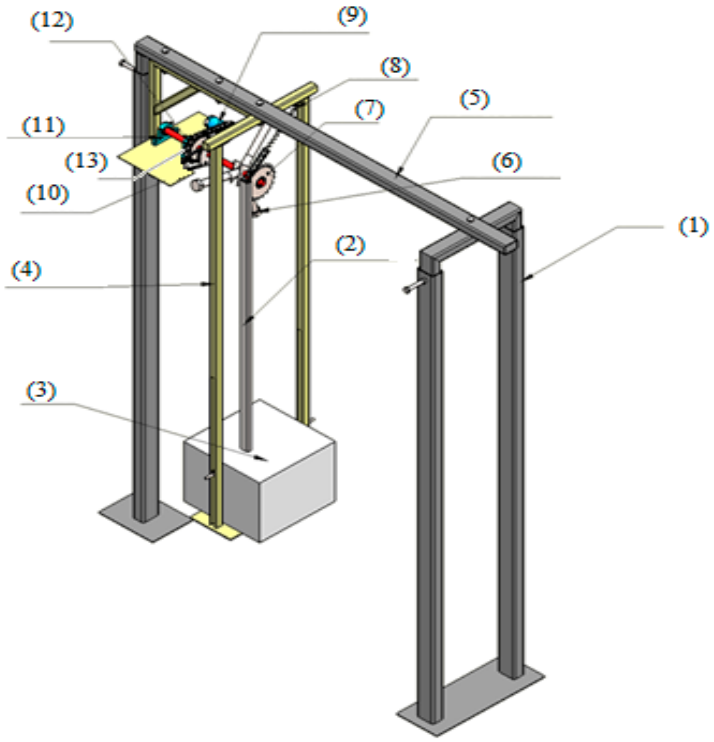

Part number	Part name
1	Adjustable base support
2	Fixed bar to the buoy
3	Floated buoy
4	Vertical linear guide
5	Movable top support
6	Equilibrium flywheel
7	Chain wheel
8	Adjustable Spring-chain system
9	Electrical generator
10	Fixed horizontal platform
11	Housed bearing unit
12	Horizontal bar Shaft
13	Belt-pulleys system
14	Chain (Figure 3)

Figure 1. Design of the MWEC prototype.

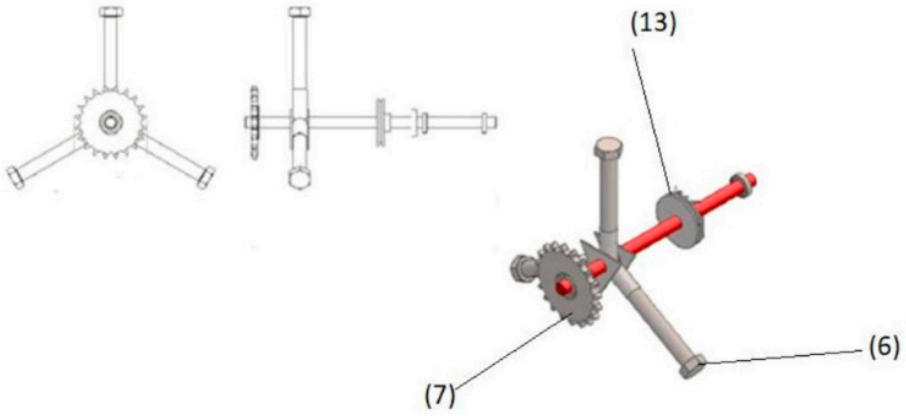

Figure 2. The MWEC horizontal transmission system.

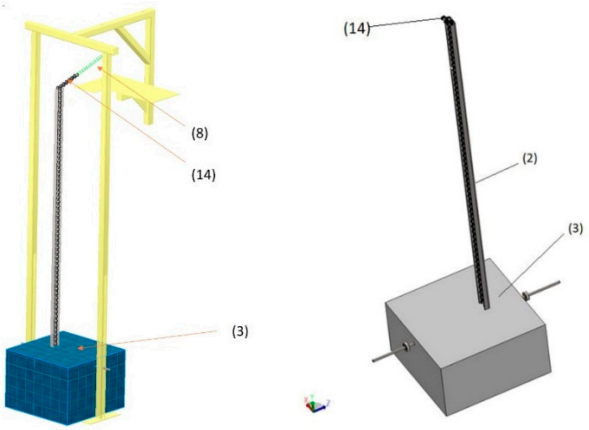

Figure 3. The PVC cubic buoy vertical transmission system for the upward movement.

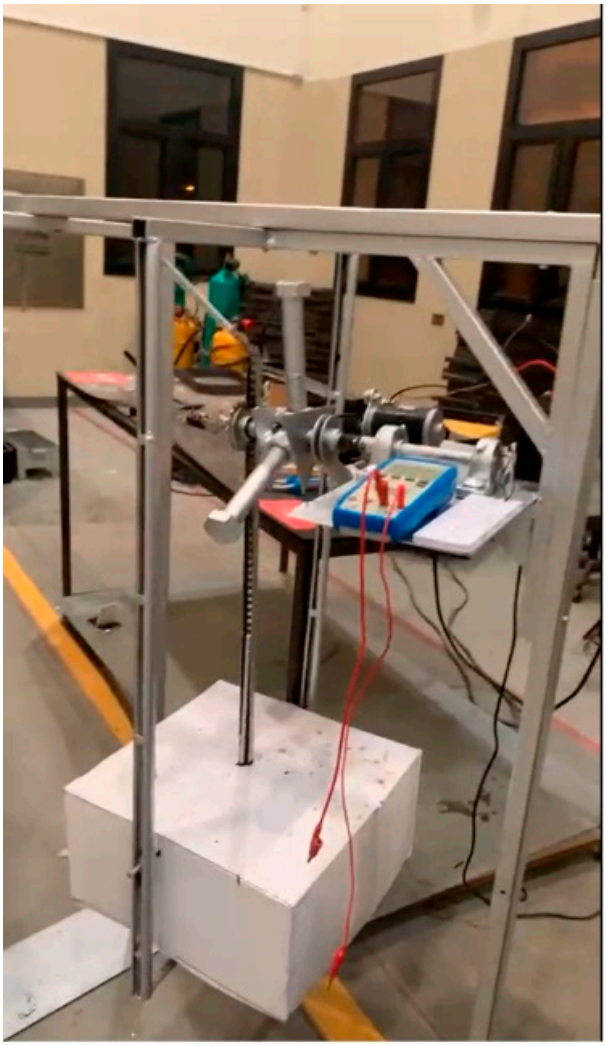

Figure 4. The prototype of the MWEC illustrates all assembled pieces.

The MWEC design in this study employs a purely mechanical rack-and-pinion, spring-restoration, and flywheel system. This approach aims for low maintenance, high robustness in high-salinity environments, and low cost. Furthermore, the system is designed for shallow waters (~1 m depth) so that larger offshore WECs cannot exploit energy in the same water depth. The novelty of the proposed MWEC is that the system is modular, and a cubic buoy design allows for easy adaptation to seasonal wave climates based on buoy volume, a feature not commonly emphasized in standard point absorber designs.

The buoy is a cubic shape formed from Polyethylene with characteristics illustrated in Table 1.

Table 1. Different buoy characteristics used in the MWEC.

Buoy	Volume (cm^3)	Mass (kg)	Dimensions (cm)
V1	6000	0.6	10 × 20 × 30
V2	30,000	1.2	20 × 30 × 50
V3	72,000	3.6	30 × 40 × 60

It is important to mention that the metallic frame is vulnerable to corrosion in the high-salinity Red Sea, requiring protective measures such as resistant alloys or coatings. In this case, a polyurethane paint coating was applied to prevent corrosion, with periodic inspections needed for repair. Seabed disturbance is another major concern in shallow waters, as it can affect system performance over time and requires regular maintenance. Managing these issues is essential for the environmental sustainability and long-term reliability of the MWEC.

The Wave Resources in Neom Coast

The Red Sea waves are more dominant in the northern region [48], where Saudi Arabia's Neom shoreline is located (Figure 5). Average wind speeds for the Neom area along the northern Red Sea coast were estimated using historical data from the Windy website [54] and compared with previous studies [6,48,55].

Figure 5. Neom shoreline in Red Sea (screenshot from Google Maps) in December 2024.

The results show that peak wind speeds occur in summer (June–August), driven by dominant wind patterns and thermal rises across the Red Sea. According to Windy historical data and GFS27 estimates for the Neom coast, wind conditions are not constant, with the dominant wind speed range between 4 and 9 m/s.

To evaluate the energy production of the MWEC, an analysis of significant wave height (Hs) was carried out in the Neom surf zone at five test points in 1 m water depth. The selected locations were created and saved on the Aqualink platform, which supports monitoring efforts by providing free, publicly accessible reef and ocean data. This platform offers instant access to valuable information for researchers, scientists, and the general public worldwide (Aqualink.com).

Table 2 presents the average wind and sea wave parameters along the Neom coastline during November and December 2024 (points created using the Aqualink platform). Data

were obtained from the NOAA Global Forecast System (GFS), accessed in November and December 2024 through https://registry.opendata.aws/noaa-gfs-bdp-pds/, (accessed on 1 November 2024 and 1 December 2024).

Table 2. Average Neom coast line wind and sea wave parameters during November and December 2024.

	Week	Wind Speed (km/h)	Wind Direction (°)	Wave Height (m)	Wave Period (seconds)	Wave Direction (°)
Average per Week November 2024	Week 1	12	239	0.7	5	291
	Week 2	3.7	243	0.6	5	296
	Week 3	9.6	178	0.6	4	359
	Week 4	15.7	201	1.1	6	284
Average per Week December 2024	Week 1	25	245	1.5	6	284
	Week 2	29.3	226	1.3	4	268
	Week 3	28.2	261	1.5	5	287
	Week 4	26.3	293	2.1	6	300

The significant wave height (Hs) was calculated using the GFS weather forecast model, and the results are provided in Table 3.

Table 3. Monthly significant wave heights (Hs) in Neom coast.

Month	Significant Wave Height (Hs) (m)	Deviation (±m)
January	1.3	±0.3
February	1.1	±0.3
March	0.9	±0.3
April	0.8	±0.1
May	0.9	±0.3
June	1.0	±0.3
July	1.1	±0.3
August	1.2	±0.3
September	0.9	±0.3
October	0.8	±0.1
November	1.0	±0.3
December	1.3	±0.3

The significant wave period (Ts) was calculated based on the Global Forecast System (GFS) weather forecast model; the results are listed in Table 4.

Table 4. Significant wave period in Neom coastline.

Month	Significant Wave Period (Ts)	Deviation (±seconds)
January	6.5	± 0.5
February	6.3	± 0.5
March	6.2	± 0.4

Table 4. *Cont.*

Month	Significant Wave Period (Ts)	Deviation (±seconds)
April	6.0	± 0.4
May	5.8	± 0.3
June	5.5	± 0.3
July	5.3	± 0.3
August	5.2	± 0.3
September	5.4	± 0.3
October	5.9	± 0.4
November	6.3	± 0.4
December	6.7	± 0.5

3. Results and Discussion

3.1. Mathematical Illustration of Wave-Energy Extraction Equations

The design of the MWEC must balance buoy mass, volume, and the PTO system to optimize energy conversion efficiency, ensuring sufficient motion for power generation without excessive damping. For that reason, a simulation of the MWEC is conducted based on the equation of motion.

Stored Energy of Waves

The real sea wave may be considered as composed of many elementary waves of different frequencies and directions. This stored energy of waves is the summation of kinetic energy and potential energy. The equation of stored energy of waves could be written as Equation (1):

$$E = \frac{\rho g {H_s}^2}{16} = \rho g \int_0^\infty S(f)df \quad (1)$$

where ρ, the mass density of sea water; g, the acceleration of gravity; Hs (m): the significant wave height for Neom coastline; S(f) (m^2/Hz) is the wave spectrum; f: wave frequencies.

The current design focuses on the vertical motion of a floating buoy in response to wave action. The buoy oscillates up and down with the wave crests and troughs, following the vertical motion generated by passing waves, see Figure 6. For that reason, mathematical illustration of wave-energy extraction can be based on the work of Johannes Falnes [56] that assumes the linear theory: if the amplitudes of waves and oscillations are sufficiently small, then the dynamic equation of the buoy could be written as follows:

$$(m + A)\ddot{S}(t) + B_f\dot{S}(t) + Kr(t) * \dot{S}(t) + Cs(t) = F_e(t) + F_u(t) \equiv F_{ext}(t) \quad (2)$$

where

Fext(t) is the extracted force;
Fe(t) is the excitation force resulting from the incident wave;
Fu(t) is a force applied intentionally for control and power take-off;
m is the body's mass;
C is the stiffness: restoring-force coefficient;
A is the hydrodynamic parameter;
Bf is a mechanical loss resistance due to mechanical PTO friction and viscosity of sea water;
kr(t) is the radiation-force impulse-response function;
S(t): The excursion (the displacement of the buoy).

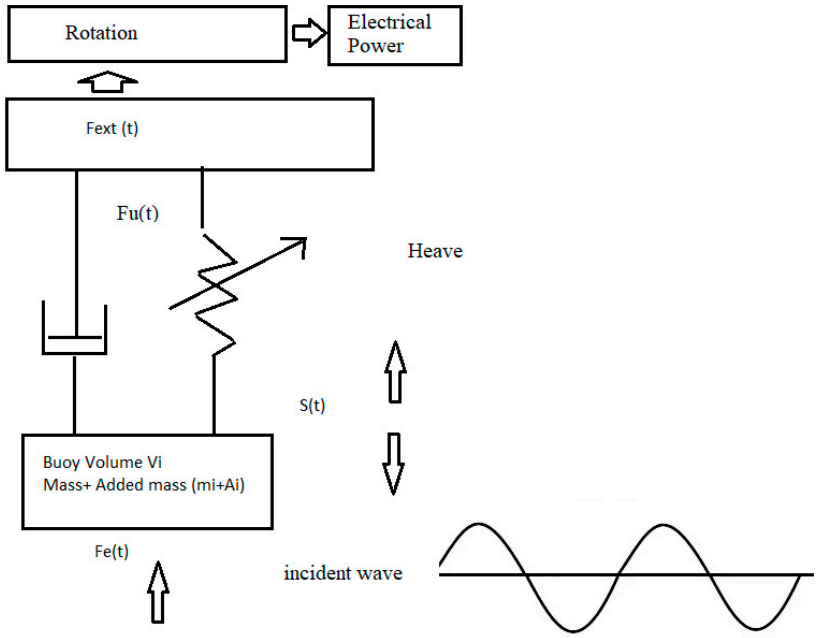

Figure 6. The vertical motion of a floating buoy in response to wave action.

The dynamic Equation (2) can be written as follows:

$$(m + A)\ddot{S}(t) = F_{ext}(t) - B_f\dot{S}(t) + Kr(t) * \dot{S}(t) + Cs(t) \quad (3)$$

where

$$A \approx Cm \cdot \rho \cdot Vi$$

where Cm is added mass coefficient in the range of 0.6–0.8.

If we combine the mechanical loss resistance due to mechanical PTO friction and viscosity of sea water 'Bf' and the radiation-force impulse-response function kr(t), Equation (3) becomes

$$\ddot{S}(t) = \frac{F_{ext}(t)}{(m + A)} - \dot{S}(t)\left(\frac{B_f}{(m + A)} - \frac{Kr(t)}{(m + A)}\right) - s(t)\frac{C}{(m + A)} \quad (4)$$

3.2. Simulation of the MWEC

Equation (4) could be written in a block diagram as shown in Figure 7:

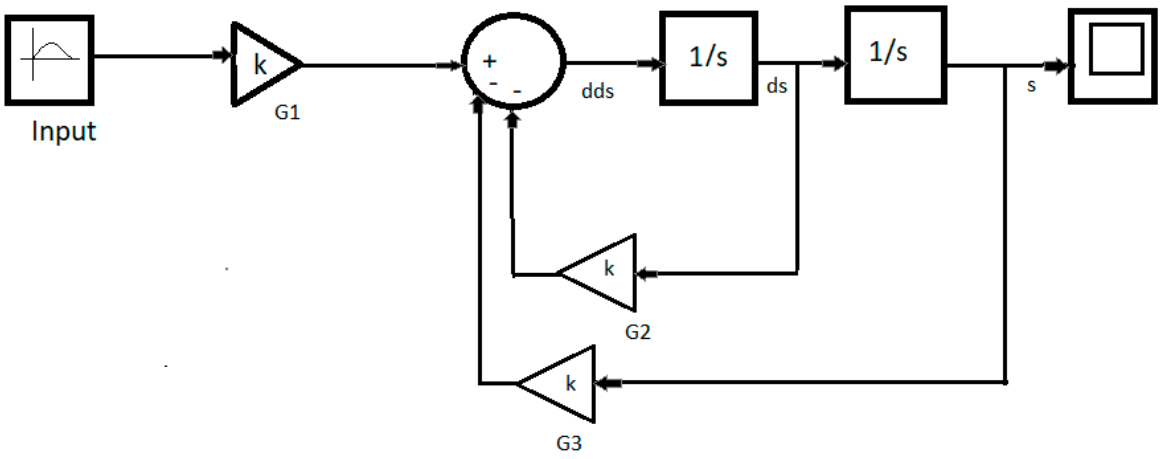

Figure 7. The block diagram of the MWEC.

The results of simulation of MWEC with consideration of three different buoys with volumes V1, V2, and V3 are shown in the following Figure 8:

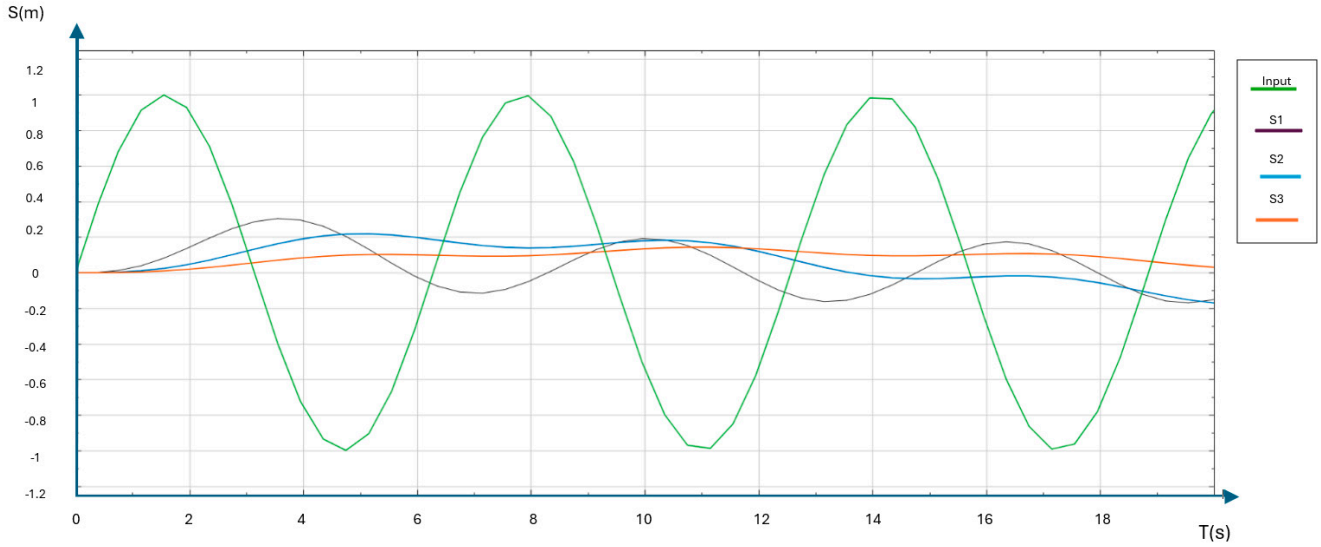

Figure 8. Simulation of MWEC amplitude S(t): S1 buoy with volume V1; S2 buoy with volume V2 and S3 buoy with volume V3.

The simulation results obtained for the three buoy volumes show that a larger volume results in a higher oscillation period, while a smaller volume leads to a higher amplitude. The larger the buoy, the lower the efficiency of the PTO system (see Figures 8 and 9). The larger the buoy volume and mass, the lower the oscillation amplitude. This suggests that increased inertia and hydrodynamic effects dampen the buoy motion. The phase shift between the different responses indicates that the system's dynamic characteristics change with buoy size (see Figures 8 and 9).

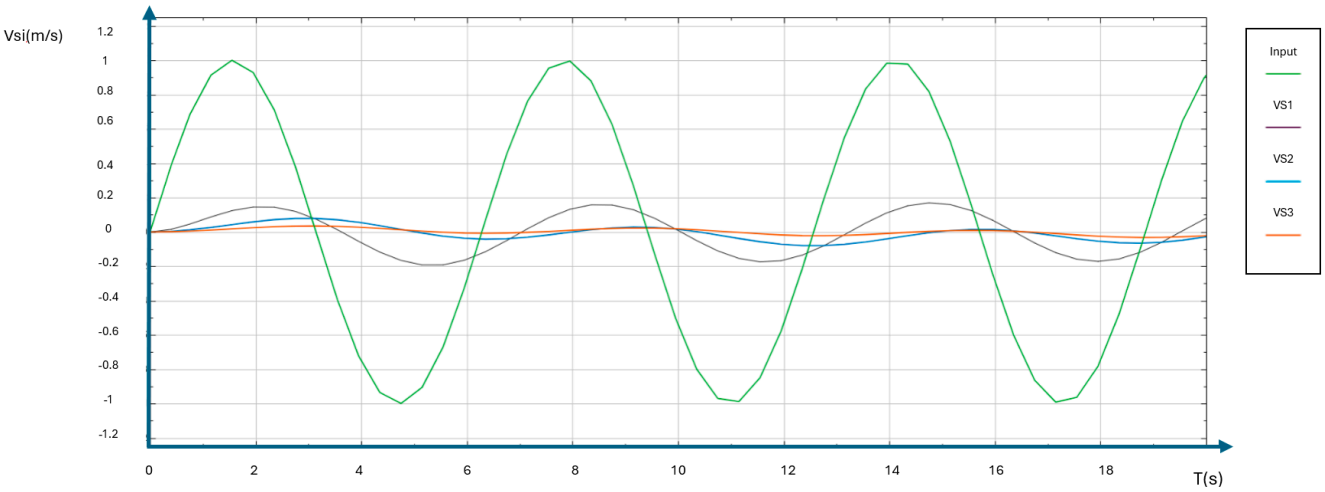

Figure 9. Simulation of MWEC velocities Vsi (t): VS1 buoy with volume V1, VS2 buoy with volume V2, and VS3 buoy with volume V3.

3.3. The Instantaneous Power

The instantaneous power Pu(t) delivered to the control and PTO system is

$$P_u(t) \equiv -F_u(t)u(t) = P_b(t) + P_d(t) \quad (5)$$

where $P_b(t)$ is the instantaneous active power;

$P_d(t)$ is the instantaneous reactive power;
u(t) is the heave velocity (the velocity of the oscillating buoy).

The wave is considered sinusoidal, for which the excitation force is $F_e(t) = F_e\cos(wt)$ and the heave velocity is $u(t) = u\cos(wt - \varphi)$

Here, φ is the phase angle between the velocity and the excitation force.

For the case of MWEC with a point absorber, the oscillating buoy generates axisymmetrical (circular) waves:

The wave period Tc:

$$T_c = \left(\frac{32\pi^4 g^{-2} V}{H}\right)^{1/4} \quad (6)$$

The output power:

$$P_c = \frac{\pi\rho g V H}{4T_c} = \left(\frac{\rho g^{\frac{3}{2}}}{8}\right)\left(\frac{V^3 H^5}{2}\right)^{1/4} \quad (7)$$

where H: wave height; V: The volume of the buoy.

The power output is directly proportional to the volume of the buoy and the wave height, and inversely proportional to the wave period. This means that a larger volume or higher wave height results in greater power output, while a longer wave period reduces the power output. Then, based on the output power equation (5), it is possible to optimize the design of the MWEC and optimize wave energy efficiency to maximize the output power Pc.

Distribution of Wave Energy over Frequency

In order to describe the distribution of wave energy over frequency, the Pierson–Moskowitz spectrum mathematical model [57] is used to describe the distribution of wave energy over frequency in a fully developed sea state. The wave spectrum in terms of the significant wave height can be written as follows:

$$S(w)\frac{\alpha g^2}{\omega^5} e^{\frac{-0.32g^2}{H_s^2\omega^4}} \quad (8)$$

The significant wave height, Hs, can be estimated by

$$H_s = 4\eta^2 = 0.21\frac{U^2}{g} \quad (9)$$

relationship between the peak or modal frequency and the significant wave height, as follows:

$$\omega_m = 0.4\sqrt{\left(\frac{g}{H_s}\right)} \quad (10)$$

The free-surface variance is given by

$$\eta^2 = \int_0^\infty S(\omega)d\omega = 0.00274\frac{U^4}{g} \quad (11)$$

where $\alpha = 8.1(10^{-3})$ and $\omega_0 = g/U19.5$.

The plot of the Pierson–Moskowitz spectrum in Figure 10 shows how wave energy density varies with angular frequency. The peak of the curve corresponds to the peak frequency ω0, where the wave energy is maximum. The comparison of the Pierson–Moskowitz spectra for December 2024 and November 2024 reveals significant differences in wave energy distribution. December 2024 had higher wave energy, shorter-period waves, and a more concentrated energy distribution compared to November 2024. These differences are likely

due to seasonal changes, increased wind speeds, and storm activity. Understanding these variations is essential for applications such as offshore engineering, ship design, and wave energy harvesting.

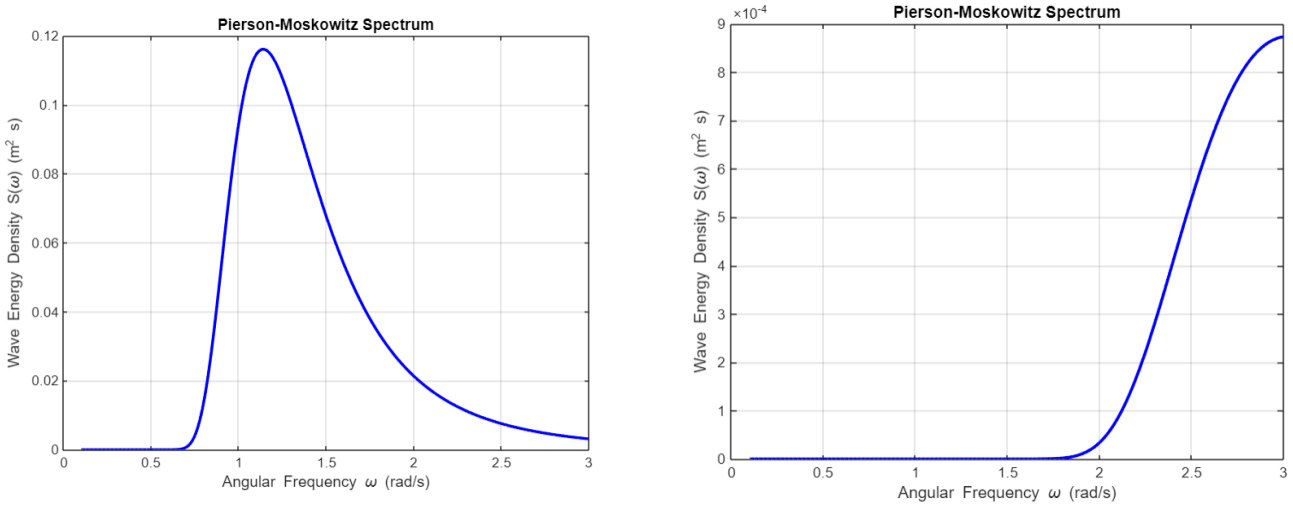

(**a**) (**b**)

Figure 10. Plot of the Pierson–Moskowitz spectrum for December 2024 curve (**a**) and November 2024 curve (**b**).

The response of the buoy can be found by solving this differential equation, which would typically require knowledge of the wave forcing function and damping characteristics of the buoy. It is expected to install the MWEC in shallow water waves. And it is important to mention that shallow water waves are affected by interaction with the floor of the sea, see Figure 1. The Energy conversion is typically achieved through a PTO system, which is a mechanism that converts the relative motion between the buoy and a fixed structure of the MWEC. The power generated from the relative motion is given by

$$P(t) = F_{wave}(t).\ V(t) \tag{12}$$

This equation gives the time-varying power output of the system.

Here P(t) is the instantaneous power generated, $F_{wave}(t)$ is the wave excitation force acting on the buoy, and v(t) is the velocity of the buoy (related to the derivative of z(t))

$$v(t) = \dot{z}(t).v(t) \tag{13}$$

To optimize the energy conversion process, the efficiency of the energy conversion would depend on the PTO mechanism and the optimum design of MWEC. The efficiency needs to be introduced into the equation of energy, and that gives

$$P_{gen} = \eta_{PTO} \cdot P(t) \tag{14}$$

That gives

$$P_{gen} = \eta_{PTO} \cdot F_{wave(t)} \cdot v(t) \tag{15}$$

where P_{gen} is the generated power; η_{PTO} is the power take-off efficiency.

The use of a buoy is essential for MWEC; the efficiency of the buoy needs to be introduced into the equation of energy, and that gives

$$P_{gen} = \eta_{PTO} \cdot \eta_{buoy}\ F_{wave(t)} \cdot v(t) \tag{16}$$

η_b is the buoy shape efficiency.

Based on the physics of wave motion, the wave energy is proportional to the square of the amplitude. Then Wave Energy Retention Coefficient (η_{RC})

$$\eta_{RC} = \eta_{PTO}\,\eta_{buoy} = (\text{Output Amplitude}/\text{Input Amplitude})^2 \quad (17)$$

where η_b is the buoy shape efficiency and η_{PTO} is the power take-off efficiency

3.4. Experimental Identification of the Energy Retention of the MWEC

To evaluate the energy retention coefficient (η_{RC}) of the MWEC system (Figure 11), three different buoys with the same material and cubic shape, with different sizes, were installed and tested. The grouped test results are shown in Table 5. Two sensing systems were used: an ultrasonic sensor to measure the output amplitude and Loadcell fixed in the PTO system to measure the output force, as shown in Table 6.

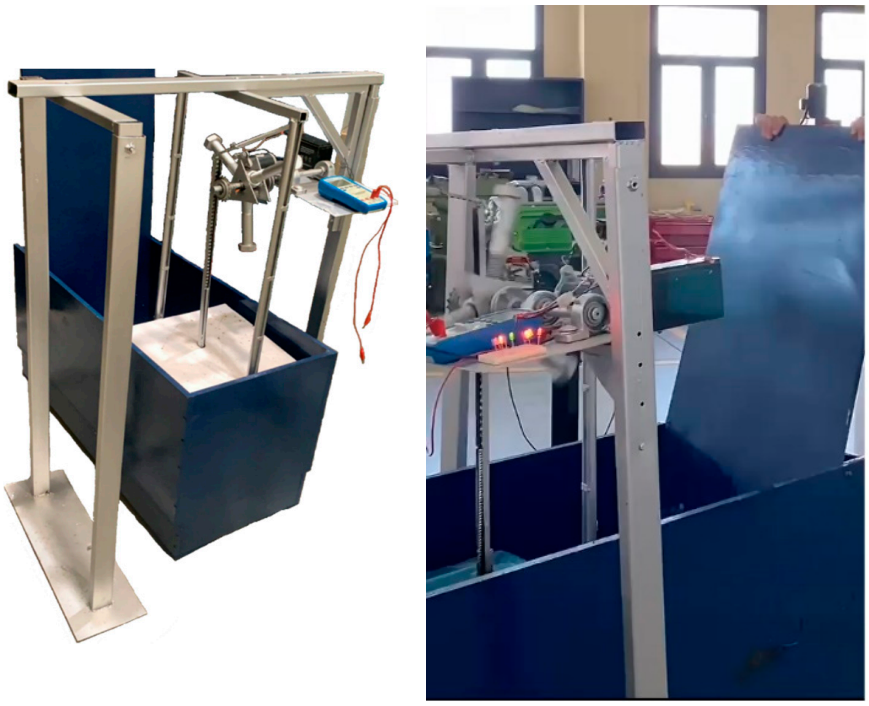

Figure 11. Experimental setup for MWEC to determine buoy volume effect and PTO retain energy coefficient.

Table 5. Experimental results of an MWEC on the wave retention amplitude on a cubic buoy with three different volumes.

Input Wave Amplitude (cm)	Avg. Output Amplitude V1 (cm)	±Error (cm)	Avg. Output Amplitude V2 (cm)	±Error (cm)	Avg. Output Amplitude V3 (cm)	± Error (cm)
20	11	±0.6	8	±0.4	6	±0.3
32	12	±0.6	10	±0.5	9	±0.5
44	18	±0.9	15	±0.8	12	±0.6
52	21.3	±1.1	20	±1.0	19	±1.0
65	30.2	±1.5	27	±1.4	24	±1.2

Table 6. Experimental results of an MWEC on the wave output force on a cubic buoy with three different volumes.

Input Wave Amplitude (cm)	Avg. Output Force V1 (N)	±Error (N)	Avg. Output Force V2 (N)	±Error (N)	Avg. Output Force V3 (N)	±Error (N)
20	12	±1.0	20	±1.6	28	±2.2
32	22	±1.8	35	±2.8	45	±3.6
44	30	±2.4	48	±3.8	62	±5.0
52	38	±3.0	58	±4.6	74	±5.9
65	50	±4.0	75	±6.0	95	±7.6

The MWEC's performance is limited by its shallow water deployment (~1 m depth), which restricts available wave energy, and by mechanical losses in its PTO system. This leads to a capture efficiency of 10–20%, which is below that of deep-water WECs. Future designs could enhance efficiency through the following:

- Optimization of buoy geometry.
- Improvement of PTO performance.
- Deployment in deeper, more energetic waters.
- Implementation of an adaptive damping PTO system to better handle irregular waves [58].

An uncertainty analysis was conducted to quantify errors in the measured output force and buoy displacement. Vertical displacement was tracked with an ultrasonic sensor, while force was measured using a load cell. The estimated uncertainties of ±5% for amplitude and ±8% for force are attributed to several factors: The natural variability of generated waves, non-sinusoidal oscillatory forces leading to inertial errors in the load cell, and fluctuating mechanical friction in the PTO's linear guides and bearings. The propagation of these errors resulted in a combined power uncertainty of ±9.4%. The consistency of this relative error across all the tests indicates a primarily systematic, rather than random, source of uncertainty.

Based on the experimental results, an overall efficiency of the PTO system with a buoy is illustrated in Table 7. The data shows that the efficiency is not constant and varies with wave amplitude and buoy mass:

Table 7. Average capture efficiency and standard deviation.

Buoy Volume	Average Efficiency (η_RC)	Standard Deviation
V1	0.1988	0.0572
V2	0.1389	0.0278
V3	0.1027	0.0268

The smallest buoy (V1 = 6000 cm^3) achieved the highest average capture efficiency (η_{RC} = 19.88%) but also showed the largest variability (σ = 0.0572) with the lowest average output power. This indicates that V1 is highly sensitive to changes in wave amplitude, which limits its suitability for higher wave conditions and makes it more appropriate for seasons with low wave energy.

The medium buoy (V2 = 30,000 cm^3) showed moderate efficiency (η_{RC} = 13.89%) with lower variability (σ = 0.0278), suggesting a more stable response compared to V1. The largest buoy (V3 = 72,000 cm^3) recorded the lowest efficiency (η_{RC} = 10.27%) but also the least variability (σ = 0.0268), indicating a more consistent performance under larger wave amplitudes, though with reduced responsiveness compared to V1 and V2. Overall, Table 8

demonstrates that larger waves deliver higher energy but drive greater vertical motion, leading to the recommendation of using smaller buoys during low wave amplitudes and larger buoys under stronger wave conditions.

Table 8. Average output power (W) for each buoy volume.

Input Wave Amplitude (cm)	Avg. Output Power V1 (W)	±Error (W)	Avg. Output Power V2 (W)	±Error (W)	Avg. Output Power V3 (W)	±Error (W)
20	8.2	±0.8	29.6	±2.8	53.3	±5.0
32	8.9	±0.8	37.0	±3.5	80.0	±7.5
44	13.4	±1.3	55.5	±5.2	106.6	±10.0
52	15.8	±1.5	74.0	±7.0	168.7	±15.9
65	22.4	±2.1	100.0	±9.4	213.1	±20.0

The rate of response differs among buoy volumes due to mass, buoyancy, and hydrodynamic damping.

- Small buoy V1 shows the highest relative output amplitude because of its low mass and inertia, allowing a quick response to wave motion.
- Medium buoy V2 provides a balanced response, with moderate amplitude and effective energy absorption.
- Large buoy V3 produces the lowest relative amplitude because higher mass and hydrodynamic effects reduce motion.

For output force, larger buoys generate higher forces despite lower displacement. Although they move more slowly, their greater mass produces stronger force output. Small buoys perform better in low-energy waves due to higher responsiveness, but excessive motion does not always translate into efficient energy conversion. For maximum force output, the large buoy performs best, making it more suitable for high-energy waves and more compatible with the PTO design, as it enables efficient conversion of force into usable energy.

As shown in Figure 12, a comparison of the theoretical and experimental results indicates that the model successfully captures the general trend of increasing output power with wave amplitude and buoy volume. However, a consistent discrepancy is evident, as the measured power values fall below the theoretical predictions. The smallest buoy shows the closest agreement with the model, while the deviation grows more pronounced for larger buoys. This is primarily attributed to energy dissipation mechanisms not accounted for in the theoretical model, such as frictional losses, shallow-water turbulence, and mechanical losses in the PTO system.

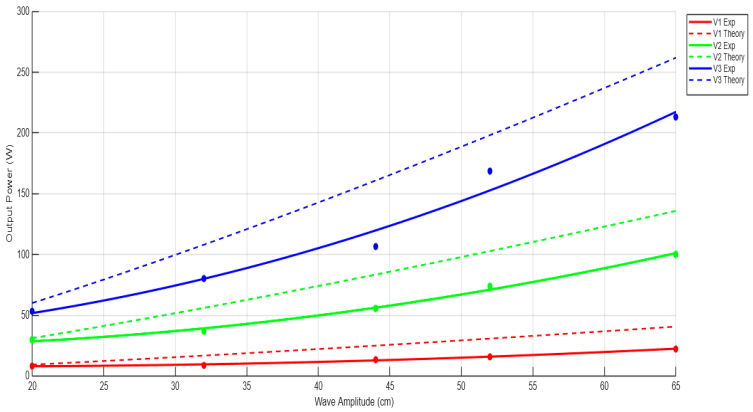

Figure 12. Comparison of experimental and theoretical output power for different buoy sizes.

The MWEC prototype in this study, with an approximate efficiency of 10–20%, represents a low-cost and mechanically simple option for shallow-water deployment. Its performance contrasts with established technologies like the Pelamis attenuator and Pico Plant oscillating water column (OWC), which achieve higher efficiencies of 20–30% and 20–40%, respectively, and power ratings in the hundreds of kilowatts. However, these systems involve greater mechanical complexity, higher maintenance, and a requirement for deep water. Similarly, point absorbers like the Power Buoy achieve moderate efficiency (15–25%) with proven designs, while large overtopping devices such as the Wave Dragon can generate several megawatts but require massive structures, unique sites, and deep water. This comparison highlights a core trade-off in wave energy: higher efficiency and output often demand increased complexity, deep-water sites, and higher installation and maintenance costs.

The MWEC prototype uses a PVC buoy for its lightweight properties and sufficient resistance. However, long-term deployment in the Red Sea demands materials with superior UV resistance and structural durability under cyclic loading. While alternatives like fiber-reinforced composites or marine-grade aluminum offer greater strength-to-weight ratios and longevity, they come at a higher cost. For this study, PVC's characteristics are suitable, but future designs using denser materials must account for the resulting changes in the buoy's dynamic response.

4. Conclusions

This study confirms the technical feasibility and performance potential of deploying a PVC-based Mechanical Wave Energy Converter (MWEC) along the southeast shoreline of NEOM (approx. 135° longitude), an area characterized by favorable nearshore wave conditions. Shallow waters (~1 m deep) in the surf zone were identified as suitable for MWEC installations, enabling low-cost deployment with minimal environmental disruption.

Three PVC cubic buoys of varying volumes—6000 cm^3 (V1), 30,000 cm^3 (V2), and 72,000 cm^3 (V3)—were experimentally assessed in conjunction with a mechanical power take-off (PTO) system. The results showed that energy retention decreased with increasing buoy volume, with efficiencies of ~20% for V1, ~14% for V2, and ~10% for V3. Despite its lower efficiency, the largest buoy (V3) achieved the highest energy capture, generating up to 213 W at a 65 cm average wave amplitude—highlighting its potential for energy-rich wave climates. Each buoy configuration offers distinct operational advantages:

V1 (small) demonstrates rapid responsiveness and is best suited for low-power applications and low-amplitude wave conditions.

V2 (medium) provides a balanced trade-off between responsiveness and output, making it a versatile, all-season option.

V3 (large) excels in energy capture under high-energy conditions but at the cost of reduced efficiency, suggesting its use in energy-intensive deployments.

To supply meaningful power for NEOM, the MWEC system would be deployed in modular arrays, analogous to offshore wind farms. The cumulative energy yield is substantial; for instance, approximately 5000 units would generate 1 MW of continuous power. This modular strategy offers significant practical advantages, as the system's capacity can be incrementally scaled to align with growing energy demands. Furthermore, the use of shallow-water sites reduces installation and maintenance expenses compared to deep-water alternatives. Finally, by generating power near the point of use, an MWEC farm can minimize transmission losses and avoid the high infrastructure costs associated with a single, large-scale power plant in deep water.

Based on the findings of this study, several promising directions for future work are recommended:

- First, the mechanical efficiency of the system should be enhanced by optimizing the linear movement of the buoy to reduce frictional losses in the power take-off (PTO) system.
- Second, a comparative investigation into buoy geometry to test spherical, cylindrical, and other shapes.
- Finally, multi-buoy array experiments in the NEOM surf zone are essential, as these would provide data on the system's durability, seasonal performance, and energy yield in the marine environment.

Author Contributions: Conceptualization, A.G.; methodology, A.G.; software, A.G.; writing—review and editing, A.G.; visualization, I.E., A.L. and M.A. All authors have read and agreed to the published version of the manuscript.

Funding: The authors extend their appreciation to the Deputyship for Research and Innovation, Ministry of Education, Saudi Arabia, for funding this research through project number (0153-1443-S).

Data Availability Statement: The original contributions presented in this study are included in the article. Further inquiries can be directed to the corresponding author.

Conflicts of Interest: The authors declare no conflicts of interest.

References

1. Chandrasekaran, S. Harender Power Generation Using Mechanical Wave Energy Converter. *Int. J. Ocean Clim. Syst.* **2012**, *3*, 57–70. [CrossRef]
2. AbdelMeguid, H.; Gherissi, A.; Elsawy, M.; Aljohani, Z.; Asiri, A.; Saber, M.; Fouda, A. Potential application of solar still desalination in NEOM region. *Appl. Water Sci.* **2024**, *14*, 1–14. [CrossRef]
3. Gherissi, A.; Alahmari, F.; Fadhl, M.; Asiri, A.; Alhwiti, M.; Alamri, O.; Alanisi, M.; Nasri, I. Wind turbine blades structure based on palm cellulose fibers composite material. *Epitoanyag J. Silic. Based Compos. Mater.* **2021**, *73*, 109–114. [CrossRef]
4. Falcão, A.F.D.O. Wave energy utilization: A review of the technologies. *Renew. Sustain. Energy Rev.* **2010**, *14*, 899–918. [CrossRef]
5. Wang, H.; Sun, J.; Xi, Z.; Dai, S.; Xing, F.; Xu, M. Recent Progress on Built-in Wave Energy Converters: A Review. *J. Mar. Sci. Eng.* **2024**, *12*, 1176. [CrossRef]
6. Alkhayyat, M.; Brahimi, T.; Langodan, S.; Hoteit, I. Wave energy converters: Barriers and drivers. In Proceedings of the International Conference on Industrial Engineering and Operations Management, Dubai, United Arab Emirates, 10–12 March 2020.
7. Dalton, G.; Alcorn, R.; Lewis, T. Case study feasibility analysis of the Pelamis wave energy convertor in Ireland, Portugal and North America. *Renew. Energy* **2010**, *35*, 443–455. [CrossRef]
8. Alamian, R.; Shafaghat, R.; Miri, S.J.; Yazdanshenas, N.; Shakeri, M. Evaluation of technologies for harvesting wave energy in Caspian Sea. *Renew. Sustain. Energy Rev.* **2014**, *32*, 468–476. [CrossRef]
9. Yazdi, H.; Ghafari, H.R.; Ghassemi, H.; He, G.; Karimirad, M. Wave power extraction by Multi-Salter's duck WECs arrayed on the floating offshore wind turbine platform. *Energy* **2023**, *278 Pt A*, 127930. [CrossRef]
10. Feng, Y.; Zhang, G.; Shen, Y.; You, Y.; Sun, J. Design of Duck Wave Power Generation Device Based on Wave Energy. *IOP Conf. Ser. Earth Environ. Sci.* **2021**, *696*, 012039. [CrossRef]
11. Chaplin, J.R.; Farley, F.J.M.; Rainey, R.C.T. Power conversion in the Anaconda WEC. In Proceedings of the 22nd International Workshop on Water Waves and Floating Bodies, Plitvice, Croatia, 15–18 April 2007; pp. 29–32.
12. Masuda, Y. An Experience of Wave Power Generator through Tests and Improvement. In *Hydrodynamics of Ocean Wave-Energy Utilization. International Union of Theoretical and Applied Mechanics*; Evans, D.V., de Falcão, A.F.O., Eds.; Springer: Berlin/Heidelberg, Germany, 1986. [CrossRef]
13. Ghafari, H.R.; Ghassemi, H.; He, G. Numerical study of the Wavestar wave energy converter with multi-point-absorber around DeepCwind semisubmersible floating platform. *Ocean Eng.* **2021**, *232*, 109177. [CrossRef]
14. Heo, S.; Koo, W. Dynamic Response Analysis of a Wavestar-Type Wave Energy Converter Using Augmented Formulation in Korean Nearshore Areas. *Processes* **2021**, *9*, 1721. [CrossRef]
15. van Rij, J.; Yu, Y.-H.; Edwards, K.; Mekhiche, M. Ocean power technology design optimization. *Int. J. Mar. Energy* **2017**, *20*, 97–108. [CrossRef]
16. Basar, M.F.; Ab Rahman, A.; Din, A.; Yahaya, Y.; Mahmod, Z. Design and development of green electricity generation system using ocean surface wave. In Proceedings of the International Conference on Energy and Sustainable Development: Issues and Strategies (ESD 2010), Chiang Mai, Thailand, 2–4 June 2010; pp. 1–11. [CrossRef]

17. Weinstein, A.; Fredrikson, G.; Parks, M.; Nielsen, K. AquaBuOY—the offshore wave energy converter numerical modeling and optimization. In Proceedings of the Oceans '04 MTS/IEEE Techno-Ocean '04 (IEEE Cat. No.04CH37600), Kobe, Japan, 9–12 November 2004; Volume 4, pp. 1854–1859. [CrossRef]
18. Cascajo, R.; García, E.; Quiles, E.; Correcher, A.; Morant, F. Integration of Marine Wave Energy Converters into Seaports: A Case Study in the Port of Valencia. *Energies* **2019**, *12*, 787. [CrossRef]
19. Valério, D.; Beirão, P.; da Costa, J.S. Optimisation of wave energy extraction with the Archimedes Wave Swing. *Ocean Eng.* **2007**, *34*, 2330–2344. [CrossRef]
20. Faiz, J.; Ebrahimi-Salari, M. Comparison of the performance of two direct wave energy conversion systems: Archimedes wave swing and power buoy. *J. Mar. Sci. Appl.* **2011**, *10*, 419–428. [CrossRef]
21. Chatzigiannakou, M.A.; Potapenko, T.; Ekergård, B.; Temiz, I. Numerical analysis of an Uppsala University WEC deployment by a barge for different sea states. *Ocean Eng.* **2020**, *205*, 107287. [CrossRef]
22. Tagliafierro, B.; Martínez-Estévez, I.; Domínguez, J.M.; Crespo, A.J.; Göteman, M.; Engström, J.; Gómez-Gesteira, M. A numerical study of a taut-moored point-absorber wave energy converter with a linear power take-off system under extreme wave conditions. *Appl. Energy* **2022**, *311*, 118629. [CrossRef]
23. Li, D.; Sharma, S.; Borthwick, A.G.; Huang, H.; Dong, X.; Li, Y.; Shi, H. Experimental study of a floating two-body wave energy converter. *Renew. Energy* **2023**, *218*, 119351. [CrossRef]
24. Mackay, E.; Cruz, J.; Livingstone, M.; Arnold, P.; Hassan, G.L.G. Validation of a time domain modelling tool for wave energy converter arrays. In Proceedings of the 10th European Wave and Tidal Energy Conference 2013, Aalborg, Denmark, 2–5 September 2013.
25. Dias, F.; Renzi, E.; Gallagher, S.; Sarkar, D.; Wei, Y.; Abadie, T.; Cummins, C.; Rafiee, A. Analytical and computational modelling for wave energy systems: The example of oscillating wave surge converters. *Acta Mech. Sin.* **2017**, *33*, 647–662. [CrossRef]
26. Jahangir, M.H.; Houmani, A.; Kargarzadeh, A. A theoretical assessment of energy efficiency of wave tower as an oscillating wave surge converter. *Ocean Eng.* **2024**, *295*, 116748. [CrossRef]
27. Yusop, Z.M.; Ibrahim, M.Z.; Jusoh, M.A.; Albani, A.; Rahman, S.J.A. Wave-Activated-Body Energy Converters Technologies: A Review. *J. Adv. Res. Fluid Mech. Therm. Sci.* **2020**, *76*, 76–104. [CrossRef]
28. Zhang, H.; Aggidis, G. Nature rules hidden in the biomimetic wave energy converters. *Renew. Sustain. Energy Rev.* **2018**, *97*, 28–37. [CrossRef]
29. Wu, J.; Qian, C.; Zheng, S.; Chen, N.; Xia, D.; Göteman, M. Investigation on the wave energy converter that reacts against an internal inverted pendulum. *Energy* **2022**, *247*, 123493. [CrossRef]
30. Jiang, X.; Shi, H.; Cao, F.; Zhao, Z.; Li, M.; Chen, Z. System analysis and experimental investigation of a pendulum-based wave energy converter. *Ocean Eng.* **2023**, *277*, 114300. [CrossRef]
31. Wan, Z.; Zheng, H.; Sun, K.; Zhou, K. A Model and Experiment Study of an Improved Pendulor Wave Energy Converter. *Energy Procedia* **2017**, *105*, 283–288. [CrossRef]
32. Neill, S.P.; Hashemi, M.R. Chapter 5—Wave Energy. In *E-Business Solutions, Fundamentals of Ocean Renewable Energy*; Neill, S.P., Hashemi, M.R., Eds.; Academic Press: Cambridge, MA, USA, 2018; pp. 107–140. ISBN 9780128104484. [CrossRef]
33. Brito-Melo, A.; Neuman, F.; Sarmento, A.J. Full-scale Data Assessment in OWC Pico. *Int. J. Offshore Polar Eng.* **2008**, *18*, 27–34.
34. Kerdtuad, P.; Simma, T.; Chaiamarit, K.; Visawaphatradhanadhorn, S. Establishment of a pico hydro power plant using permanent magnet synchronous generator supplied for ac microgrid. In Proceedings of the 2018 International Electrical Engineering Congress (iEECON), Krabi, Thailand, 7–9 March 2018; pp. 1–4. [CrossRef]
35. Ogata, T.; Washio, Y.; Osawa, H.; Tsuritani, Y.; Yamashita, S.; Nagata, Y. The open sea tests of the offshore floating type wave power device "Mighty Whale": Performance of the prototype. In Proceedings of the ASME 2002 21st International Conference on Offshore Mechanics and Arctic Engineering, Oslo, Norway, 23–28 June 2002; pp. 517–524. [CrossRef]
36. Hotta, H.; Washio, Y.; Yokozawa, H.; Miyazaki, T. R&D on wave power device "Mighty Whale". *Renew. Energy* **1996**, *9*, 1223–1226. [CrossRef]
37. Wu, B.; Chen, T.; Jiang, J.; Li, G.; Zhang, Y.; Ye, Y. Economic assessment of wave power boat based on the performance of "Mighty Whale" and BBDB. *Renew. Sustain. Energy Rev.* **2018**, *81*, 946–953. [CrossRef]
38. Hannon, M.J.; van Diemen, R.; Skea, J. Lost at sea or a new wave of innovation? Examining the effectiveness of the UK's wave energy innovation system since 2000. In Proceedings of the International Sustainability Transitions 2018, Manchester, UK, 12–14 June 2018.
39. Manasseh, R.; McInnes, K.L.; Hemer, M.A. Pioneering developments of marine renewable energy in Australia. *Int. J. Ocean. Clim. Syst.* **2017**, *8*, 50–67. [CrossRef]
40. Mustapa, M.; Yaakob, O.; Ahmed, Y.M.; Rheem, C.-K.; Koh, K.; Adnan, F.A. Wave energy device and breakwater integration: A review. *Renew. Sustain. Energy Rev.* **2017**, *77*, 43–58. [CrossRef]
41. Kaygusuz, E.; Soliman, A.M.S.; Mutlu, H. Wave Energy: A global overview of the current state of established companies. In Proceedings of the CISET—2nd Cilicia International Symposium on Engineering and Technology, Mersin, Turkey, 10–12 October 2019.

42. Margheritini, L.; Vicinanza, D.; Frigaard, P. SSG wave energy converter: Design, reliability and hydraulic performance of an innovative overtopping device. *Renew. Energy* **2009**, *34*, 1371–1380. [CrossRef]
43. Vicinanza, D.; Margheritini, L.; Kofoed, J.P.; Buccino, M. The SSG Wave Energy Converter: Performance, Status and Recent Developments. *Energies* **2012**, *5*, 193–226. [CrossRef]
44. Parmeggiani, S.; Chozas, J.F.; Pecher, A.; Friis-Madsen, E.; Sørensen, H.C.; Kofoed, J.P. Performance Assessment of the Wave Dragon Wave Energy Converter Based on the EquiMar Methodology. In Proceedings of the 9th European Wave and Tidal Conference, Southampton, UK, 5–9 September 2011.
45. Langodan, S.; Cavaleri, L.; Viswanadhapalli, Y.; Hoteit, I. The Red Sea: A Natural Laboratory for Wind and Wave Modeling. *J. Phys. Oceanogr.* **2014**, *44*, 3139–3159. [CrossRef]
46. Hwang, I.-K.; Lee, M.; Han, J.; Choi, J. Wave height measurement scheme using wave detector based on convolutional neural network and PPM calculator with ocean wave images. *Int. J. Nav. Arch. Ocean Eng.* **2023**, *15*, 100542. [CrossRef]
47. Langodan, S.; Cavaleri, L.; Pomaro, A.; Vishwanadhapalli, Y.; Bertotti, L.; Hoteit, I. The climatology of the Red Sea–part 2: The waves. *Int. J. Clim.* **2017**, *37*, 4518–4528. [CrossRef]
48. Elshinnawy, A.I.; Lobeto, H.; Menéndez, M. Changing wind-generated waves in the Red Sea during 64 years. *Ocean Eng.* **2024**, *297*, 116994. [CrossRef]
49. Têtu, A. Power Take-Off Systems for WECs. In *Handbook of Ocean Wave Energy*; Pecher, A., Kofoed, J., Eds.; Ocean Engineering & Oceanography, Volume 7; Springer: Cham, Switzerland, 2017. [CrossRef]
50. Waskito, K.T.; Geraldi, A.; Ichi, A.C.; Yanuar; Rahardjo, G.P.; Al Ghifari, I. Design of hydraulic power take-off systems unit parameters for multi-point absorbers wave energy converter. *Energy Rep.* **2023**, *11*, 115–127. [CrossRef]
51. Srisuwan, C.; Rattanamanee, P.; Rattanapitikon, W. Analytical formula for estimation of surface wave power with application in the coastal ocean of Thailand. *Ocean Eng.* **2020**, *204*, 107273. [CrossRef]
52. Available online: https://aqualink.org (accessed on 1 December 2024).
53. Pecher, A.; Kofoed, J.P.; Larsen, T.; Marchalot, T. Experimental Study of the WEPTOS Wave Energy Converter. In Proceedings of the ASME 2012 31st International Conference on Ocean, Offshore and Arctic Engineering, Rio de Janeiro, Brazil, 1–6 July 2012; Volume 7, pp. 525–534. [CrossRef]
54. Available online: https://windy.app/map/#c=28.05487,34.70381&z=10 (accessed on 1 December 2024).
55. Langodan, S.; Cavaleri, L.; Vishwanadhapalli, Y.; Pomaro, A.; Bertotti, L.; Hoteit, I. The climatology of the Red Sea—Part 1: The wind. *Int. J. Clim.* **2017**, *37*, 4509–4517. [CrossRef]
56. Falnes, J. A review of wave-energy extraction. In *Marine Structures*; CRC Press: Boca Raton, FL, USA, 2007; Volume 20, pp. 185–201. [CrossRef]
57. Katopodes, N.D. Chapter 2—air-water interface. In *Free-Surface Flow*; Katopodes, N.D., Ed.; Butterworth-Heinemann: Oxford, UK, 2019; pp. 44–121. ISBN 9780128154878. [CrossRef]
58. He, R.; He, G.; Jing, P.; Luan, Z.; Liu, C. Adaptive Damping PTO Control of Wave Energy Converter for Irregular Waves Supported by Wavelet Transformation. *Energies* **2025**, *18*, 3328. [CrossRef]